CURRENT STATUS ON ESS MEDIUM ENERGY BEAM TRANSPORT

I. Bustinduy*, M. Magan, F. Sordo, ESS-Bilbao, Spain
R. Miyamoto†, ESS, Sweden

Abstract

The European Spallation Source, ESS, uses a high power linear accelerator for producing intense beams of neutrons. During last year the ESS linac cost was reevaluated, as a consequence important modifications were introduced to the linac design that affected Medium Energy Beam Transport (MEBT) section. RFQ output beam energy increased from 3 MeV to 3.62 MeV, and beam current under nominal conditions was increased from 50 to 62.5 mA. The considered MEBT is being designed primarily to match the RFQ output beam characteristics to the DTL input both transversally and longitudinally. For this purpose a set of eleven quadrupoles is used to match the beam characteristics transversally, combined with three 352.2 MHz CCL type buncher cavities, which are used to adjust the beam in order to fulfill the required longitudinal parameters. Finally, thermo-mechanical calculations for adjustable halo scraping blades, with significant impact on the HEBT, will be discussed.

INTRODUCTION

The European Spallation Source (ESS) is a neutron source currently under construction in Lund, Sweden. The design and operation of the proton linac of ESS, which will ultimately produce a 5 MW beam power, is imposing challenges in various aspects of accelerator science and engineering. The main focus of this paper is the medium energy beam transport (MEBT), located between the RFQ and DTL.

Including all required devices in a relatively short space imposes significant challenges not only on engineering design of components but also beam physics since good beam quality and good matching to the DTL must be achieved under engineering limitations and strong space charge force. Table 1 shows selected parameters of the ESS MEBT. This paper presents status on works of beam physics and engineering component designs for the MEBT. However, due to the limitation in space, only the recent works for the scraper system are presented in detail and status on the rest of works is summarized in the next section.

Table 1: Selected ESS MEBT Parameters

Parameter	Unit	Value
Beam energy	MeV	3.62
Peak beam current	mA	62.5
Average beam power	kW	9.05
Beam pulse length	ms	2.86
Beam pulse repetition rate	Hz	14
Duty cycle	%	4
RF frequency	MHz	352.21

SUMMARY OF ESS MEBT STATUS

Lattice Design and Beam Physics

Figure 1 shows the present MEBT layout as well as the power beam density contours. A substantial effort has been made to construct a lattice with good matching to the DTL and good beam quality, while housing the chopper and other necessary devices [1]. The impacts from various lattice element errors have been studies as a part of the campaign to find tolerances of the lattice element errors throughout the entire ESS Linac [2]. A further detailed beam dynamics calculation including effects such as multipole components of a quadrupole and the field profiles of the buncher cavity and quadrupole will be conducted in near future.

To ensure a good chopping efficiency, the optics and beam dynamics during the chopper operation must be studied in addition to the nominal case [1]. Given the rise and fall time of the chopper is presently specified as ~10 ns, which is longer than the bunch spacing of 2.84 ns (inverse of 352.2 MHz), there are a few *partially-chopped* bunches. These bunches have large trajectory excursions but not entirely intercepted by the chopper dump, and thus raise a concern of beam losses. The dynamics and beam losses of these bunches are studied in detail and it is ensured that the losses are acceptable [3,4].

In Fig. 1, three locations at 0.85, 2.19, and 3.39 m correspond to the scrapers. The use of the scrapers for the ESS Linac has been studied in detail [1,3–5]. The scrapers not only improve the beam quality in the nominal condition but also efficiently remove halos in the RFQ output, in case the sections upstream of the MEBT produce a bad quality beam [1] and improve the situation of the beam losses due to the partially-chopped bunches [3]. The locations of the scrapers are determined to optimize these three functions under the mechanical constraints. An analysis of the location optimization of the scrapers is presented in a following section. An ability of a scraper is estimated with a thermo-mechanical calculation and this gives an important input to the beam dynamics calculation. This is also presented in a following section.

Component Design and Prototyping

In order to proceed with detailed engineering phase some constrains have to be taken into account: The elected beam pipe is the standard *DN35*. This beam pipe gives an upper limit of 18.4 mm radius for the beam aperture and also determines aperture for the rest of the foreseen devices (quadrupoles, bunchers, etc.). Constituting thus, the backbone of the MEBT engineering design.

* ibon.bustinduy@essbilbao.org
† ryoichi.miyamoto@esss.se

ISBN 978-3-95450-173-1

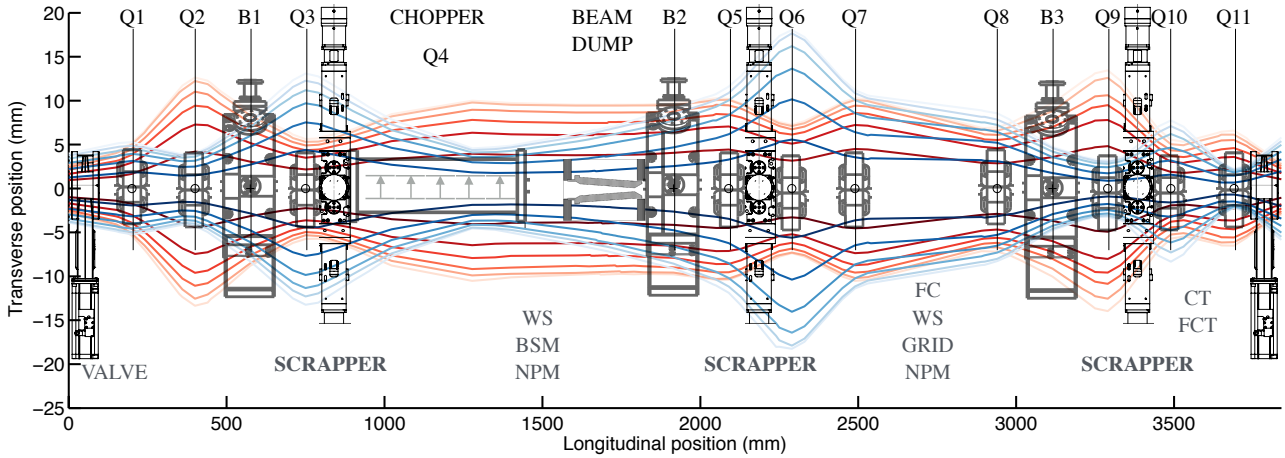

Figure 1: ESS MEBT 2014.v1 layout; comprised of 11 quadrupoles 3 bunchers and 3 scrapers. Power density contours for x (*red*) and y (*blue*) are represented from dark (10^3 W) to light (10^{-2} W) beam power contour lines extracted from TRACEWIN. Both axis are expressed in mm.

One of the main purposes of the ESS MEBT is to house a fast chopper. The bunches produced during the transient times of the IS and LEBT, positioned in the head and tail of a pulse and anticipated with a time scale of a few µs, are likely to have wrong parameters and hence a higher risk of causing beam losses [6]. In a worst case scenario, machine protection system also expects a 1 ms train of bunches to be deflected against the beam dump. In order to prevent excessive heat deposition on the beam dump, Ion source magnetron should be used as an actuator [7]. Once required rise time has been relaxed significantly (10 ns), an approach based on fast high voltage switches seems to be the most reliable approach; due to its resistance to beam spills and much simpler fabrication [8].

For this MEBT layout, an optimization of the magnetic design of the quadrupoles is being taking place in order to fulfill with following specifications: Ø41 mm aperture, $\int B = 2.5$ T with 100 mm maximum physical size (length) and ~20 G.m deflection for the steerers. This magnetic design is closely linked to the optical layout and the imposed mechanical constraints. In particular, this design has to accommodate strip-line BPM as well as the required four fiducial points at the top of the yoke. The field quality must be cross examined by particle tracking simulations, and it is especially important for these devices because the steering dipoles are integrated inside the quadrupoles.

For the longitudinal plane, a new electromagnetic design is in progress to fulfill new specifications of the foreseen three CCL type buncher cavities. The increasing transported beam energy and current affect primarily to transit time factor and required effective voltage, which increases up-to 146 kV for the last buncher under nominal conditions. In order to reach required performance in the available space, optic design has been adapted to allow a lower aperture for the bunchers (Ø29 mm).

SCRAPERS LOCATION

The use of scrapers before entering DTL tanks is strongly recommended to avoid emittance growth and halo development in high-intensity linacs [9]. In our current design, beam should be scraped in the both transverse plane at each location. For this, 4 stepping motors are needed per locations. The scrapers will be used during nominal operation, therefore integrated in the interlock system in order to avoid interaction with the beam core. The position of the beam will be provided by a beam position monitor (BPM) positioned as close as possible and the movement has to be limited. In addition, the temperature can be measure in the scraper and also the charge deposition.

Procedure

Although a simple method was use to place these scrapers [5]. It seems necessary to identify a procedure to find the best possible locations to scrape halo particles while maximizing core particles transmission, in case scraper locations could be optimized for present or forthcoming MEBT layouts.

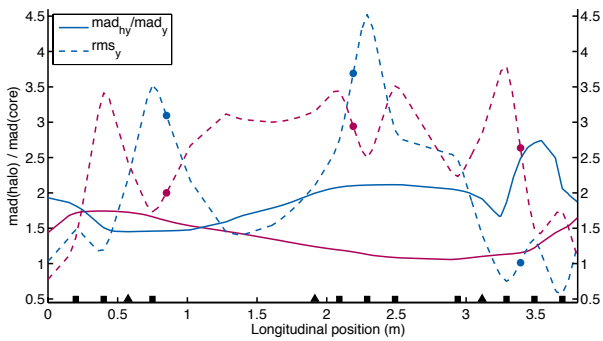

Figure 2: Beam σ beam envelopes (*dashed line*), and quadratic mean ratios (*solid line*) for x and y projections along MEBT.

ISBN 978-3-95450-173-1

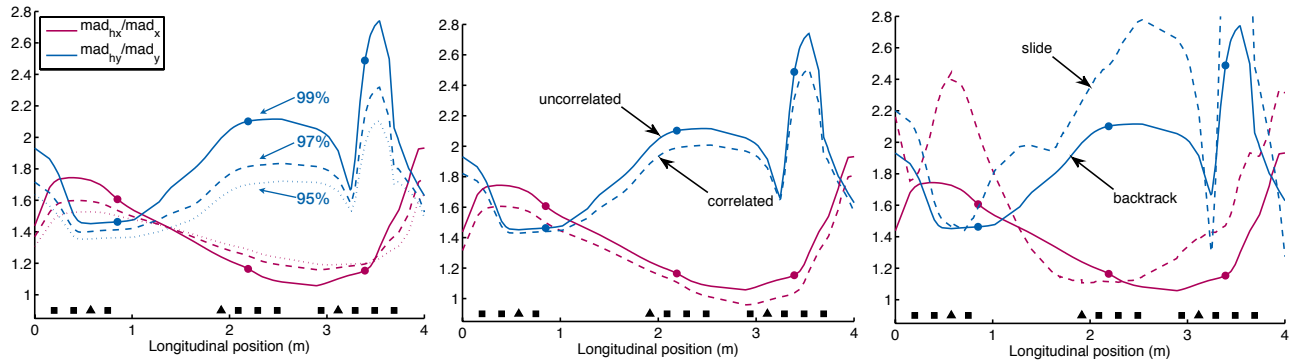

Figure 3: *Left frame:* Study of different threshold levels. *Middle frame:* Comparison between correlated or uncorrelated x/y approach. *Right frame:* Comparing tracking approach with slide by slide analysis.

Considering the mean deviation as a robust measure of population of a univariate distribution, representing the ratio of the population of particles that conform the halo respect to the particles from the core, one can identify the best possible locations to scrape halo particles maximizing *core* particles transmission. For a sample size n, the mean deviation (MAD) is defined by the following formula:

$$\mathrm{MAD} = \frac{1}{n}\sum_{i=1}^{n} |x_i - \bar{x}|, \qquad (1)$$

Particle distribution at the end of the ESS *warm linac* section [1] is scrutinized in each transverse plane. From there, particles that belong to halo are identified as those lying above a particular threshold (99% emittance). Those particles which we intend to remove, are backtracked along this medium energy beam section of the linac.

Figure 2 represents beam root mean square (RMS) in dashed lines along the MEBT. Simultaneously, the ratio of *halo/core* populations is represented when core bunch is considered within 99% emittance as solid lines. In this Figure x dimension is represented in red, while blue is used for y projection. Colored circles represent current location for scrapers (x/y). Black squares and triangles represent location of quadrupoles and bunchers respectively along the line, as presented in Fig. 1.

Robustness Testing

In order to test this method, different variations have been studied. In particular, a modification of the *threshold level*, that is used to determine the fraction of particles considered within *core*, or belonging to *halo* region could mislead the actual optimum location. For that, three different levels have been considered (see Fig. 3 left frame) 99, 97, and 95%. Here, little differences can be appreciated in the overall pattern. Another variation is to evaluate the net effect of considering x and y distributions completely independent each other, compared to the correlated case. As Fig. 3 middle frame shows, a smoothing effect arises again, but the same patterns can be identified.

[1] MEBT and DTL versions are *2014.v1* and *v86* respectively

Finally, an *slice by slice* approach is studied, in this alternative approach, beam through the MEBT is sliced and core and halo populations identified for each slide. Figure 3 right frame, represents the backtracking approach (solid lines) and slice by slice approach (dashed lines). Compared to the presented approach, where beam evolution along the warm linac accelerator is considered, slide by slide approach does not take into account core particles, that might become part of the halo downstream. It is remarkable that in both approaches same pattern arise. In particular, the best possible location for y-axis (highest values) is identified at *Q10* for both cases. Other possible good locations seem to be slightly shifted respect to *backtracking* approach. For instance, in vertical plane it can be identified a good location near *Q7*, while horizontal plane slits optimal position can be identified near *Q2*.

Discussion

Table 2 compares obtained optimal locations using the method explained above, with nominal locations, where mechanical constrains have been taken into account. From here, we can identify scraper #2 and scraper #3 as good locations to clean particles in the y dimension. while, x projection cleaning could be more effective with scraper #1. Considering mechanical constrains, performance of scraper #1 could be increased by placing it closer to the entrance. This could be achieved by exchanging positions with Wire-Scanner #1. But this, will have an impact on the beam instrumentation and the studied phase space cleaning performance, in case the beam out of the RFQ has a too populated halo.

Table 2: Beam Population Ratios per Scraper Potential Location

	Optimum		Nominal	
Scraper	z (m)	RATIO (x/y)	z (m)	RATIO (x/y)
#1	0.36	1.74/1.57	0.85	1.61/1.46
#2	2.45	1.09/2.12	2.19	1.16/2.10
#3	3.54	1.29/2.74	3.39	1.15/2.48

ISBN 978-3-95450-173-1

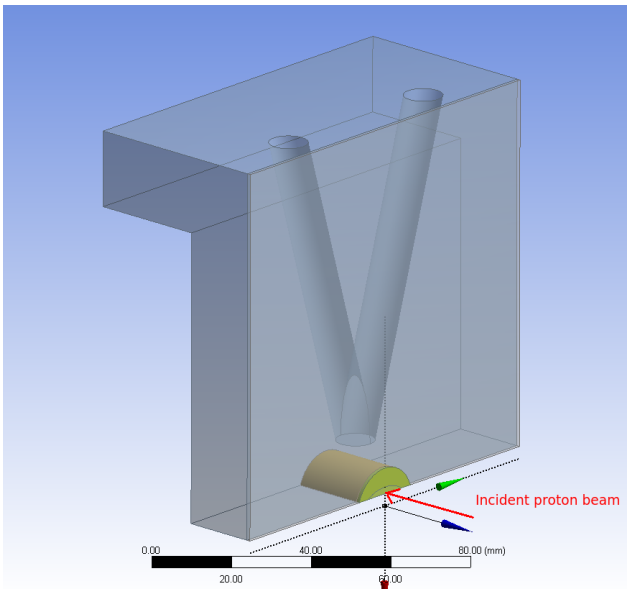

Figure 4: 3D representation of the geometry.

THERMO-MECHANICAL PROBLEM

Under the new beam parameters, the beam has a peak intensity of 62.5 mA at 3.62 MeV, with a repetition rate of 14 Hz, and a pulse length of 2.857 ms. This is a significant increase over previous conditions (50 mA and 3 MeV). In fact, the new beam conveys 50% more energy per pulse. Thus, for any given fraction of the beam that a design aims to stop, the loads are far greater than in the previous case. As a reference, each of the pulses now carry 643 J.

Considering the nominal location for each scraper (see Fig. 1), which fulfill mechanical constrains. In order to study the thermo-mechanical limits of the proposed design, the *extreme case* of a $\sigma_y = 1.01$ mm will be considered. This last scraper deals with the more focused beam in the y dimension. The area of the beam in this particular location is $\approx 15 \times 6 = 90\,\text{mm}^2$, which highlights the concentration of the beam.

In order to scrape this highly concentrated beam, the geometry presented in Fig. 4 is proposed. This L-shaped piece embraces a small cylinder of a highly temperature resistant material where the protons hit. In this case, tungsten is studied as the base candidate, although other materials have shown superior performance on theory, their manufacturability is unclear. The piece is cooled by an V-shaped cavity. While this offers a much lower cooling efficiency than an U-shaped one, as there is much less area near the area to cool, it is also much easier to manufacture, and means that the scraper can be manufactured in one piece, as opposed to the two welded pieces design an U-shape requires. Thus, removing welded parts inside vacuum, leakage problem reduces significantly, which is a remarkable reliability advantage. For these calculations, an uniform heat transfer coefficient of $10\,000\,\text{W}/(\text{m}^2 \cdot \text{K})$ is assumed.

Table 3: Summary of the Results (Each Blade)

Insertion (σ)	Max. heat flux (W/cm^2)	Max Temp (°C)	Max Stress (MPa)
3.48	1700	50.0	25.5
3.29	3350	80.0	53.2
3.1	4810	105.3	75.9
3.02	5550	120.4	90.3
2.97	6740	138.8	107
2.81	9130	185.7	149
2.67	12900	249.1	208
2.54	17600	334.0	283

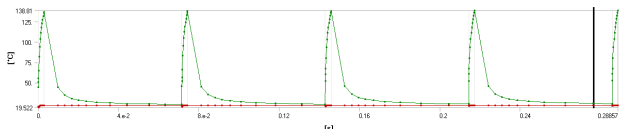

Figure 5: Peak temperature over time.

Methodology and Tools

An ANSYS™ Workbench simulation is set up with the geometry described previously. A transient thermal simulation is performed, where the heat load is given as a surface heat flux matching the beam profile during the beam pulses, and considered zero outside of them. The properties considered for the tungsten are temperature-dependent.

Results

The temperature over time, max temperature and the stress at the time of maximum temperature (pulse ending) have been calculated in several scenarios, characterized by the proximity of the scraper edge to the center of the beam in terms of the times of its RMS (σ) value. Thus, as this value decreases, the scraper is nearer the beam, and stops a larger fraction of it. A summary of all data is given in Table 3. An example of the maximum temperature over time is given in Fig. 5, for $\sigma = 2.8$, with the qualitative behavior of the temperature being the same in all cases. As all the heat deposition takes place along the 2.86 ms pulse length, there is not enough time for any significant cooling. Thus, it can be concluded that no enhancement in the cooling conditions (increase of heat transfer coefficient, area cooled, or proximity) will be of any use. As an example of the temperature field distribution, Fig. 6 represents the temperature at the end of the pulse for $\sigma = 2.8$.

Stresses are heavily located in the corner, as it suffers sudden, localized temperature increase, and is subject to thermal stress. An example of the distribution is given in Fig. 7.

It is necessary to remark that the values presented in Table 3, consider a 100 MPa stress limit in the tungsten without entering a detailed fatigue stress analysis, it can be inferred that the usage of this design is valid for values up-to $\sigma = 2.8$, or 0.15% beam scraped per blade, which would imply a 54 W, shared among the 4 blades that conform the last scraper.

ISBN 978-3-95450-173-1

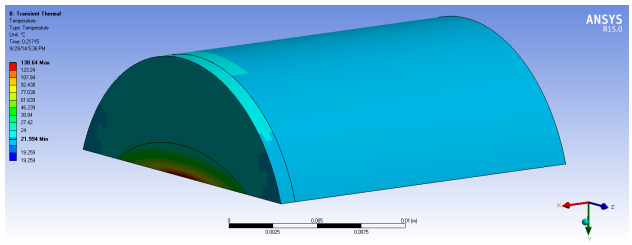

Figure 6: Temperature distribution at the end of the 2.86 ms, 14Hz repetition rate pulse.

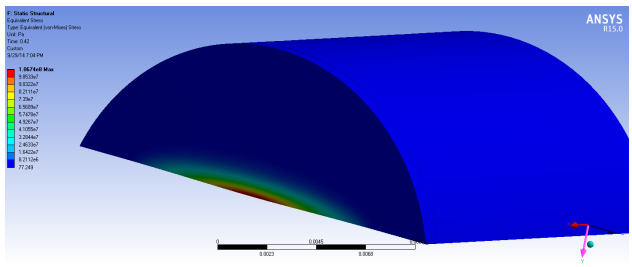

Figure 7: Stress distribution at the end of the 2.86 ms, 14Hz repetition rate pulse.

Finally, Fig. 8 presents the studied extreme case of σ = 1.01 mm in red accompanied with wider beam footprint results. σ = 3.5 mm (blue) and 7 mm (green). For a given beam cross-section, the parameter that fixes the performance requirement is the amount of beam to be scraped, which can be represented by either the percentage of the power to be scraped, or by the RMS (σ) value at which the beam is cut.

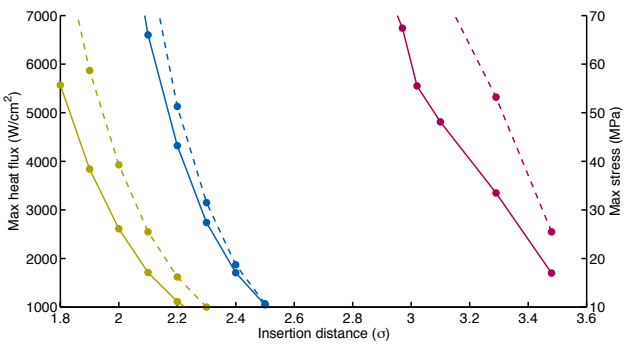

Figure 8: Max heat flux represented against insertion distance in solid lines, for three different beam footprints σ = 1.01 (red), 3.5 (blue) and 7 mm (green). Max Stress is also presented as dashed lines.

CONCLUSIONS

Overall presented method provides optimal locations for the scrapers that are in good agreement with the nominal positions (see Table 2), where, mechanical constrains, beam instrumentation needs and beam cleaning effects were also considered. This results are in good agreement with previously presented locations [5] and confirm that a typical scheme using a set of collimators separated by a fix value of phase advance, such as two scrapers separated by 90 degrees, may not be optimum for the MEBT due to the strong space charge force.

The mechanical design has been simulated under different conditions, namely, loads depending on the fraction of beam scraped, and the stress and temperature results have been analyzed. The induced stress in the beam scraper has been observed to be directly correlated to the maximum surface heat flux. Therefore, the design seems viable for values below 7000·W/cm^2. Thus, particles can be removed near 3σ as required [5], even in the highest concentration conditions. In case these collimation blades are used in the other expected locations, where beam concentration is relaxed, a higher fraction of beam can be removed safely.

ACKNOWLEDGMENT

The authors strongly thank A. Ponton, E. Sargsyan and S. Gammino and very specially the rest of ESS and ESS-Bilbao teams.

REFERENCES

[1] R. Miyamoto et al., in Proc. of IPAC'14, THPME045.
[2] M. Eshraqi et al., in Proc. of IPAC'14, THPME043.
[3] R. Miyamoto et al., in Proc. of LINAC'14, MOPP039.
[4] R. Miyamoto, in Proc. of HB'14, MOPAB18.
[5] R. Miyamoto et al., in Proc. of HB'12, WEO3A02.
[6] M. Comunian et al., in Proc. of HB'12, TUO3B01.
[7] A. Nordt et al., in Proc. of IPAC'14, MOPME045.
[8] S. Varnasseri et al., DIAG-00-CH01-ESS-00-DOC.
[9] F. Gerigk, et al., in Proc. of LINAC'02, TH103.

ISBN 978-3-95450-173-1